Supplementary Note

Supplementary Figure 1 Phenotyping pipeline

All mice were subjected to the same phenotyping pipeline.

Supplementary Figure 2 Pairwise identity by descent in 2,073 mice

Estimates of identity by descent (IBD) for all pairs of mice. Z0 on the horizontal axis shows the proportion of IBD = 0; Z1 on the vertical axis shows the proportion of IBD = 1. Each point represents one pair of mice among the 2073 mice in the sample. Points coloured in red represent pairs of mice in which at least one has a) greater proportion IBD (PI_HAT = Z2 + 0.5 x Z1) than 0.5, or b) Z1 greater than 0.75, or c) Z0 smaller than 0.25 with another mouse in the sample, indicative of IBD higher than second degree relatives. All other pairs of mice were coloured in blue. 135 mice meet the above conditions and were removed from subsequent analyses.

Supplementary Figure 3 Principal component in 1934 mice (after removing related animals)

Principal components 1 to 5 plotted against each other, from PCA on LD-adjusted GRM of 1934 mice used in GWAS.

Supplementary Figure 4. Quantile quantile plots for ten phenotype mapped in the CFW mice.

Each plot shows the relationship between expected and observed results (expressed as the negative logarithm (base 10) of the P-value (-log10). Plots are titled with the name of the phenotype, full details of which can be found in Supplementary Table 1. The genomic inflation factor (lambda), the ratio of the median of the empirically observed distribution of the test statistic to the expected median, is shown at the top of each plot.

Supplementary Table 1: List of phenotypes

This table lists the 200 measures from 18 assays used for the genetic analysis. Each as been assigned a unique name used to describe it in subsequent Supplementary tables. We report the number of mice generating data for the analysis (after exclusion of outliers), the mean and standard deviation for all animals and males and females separately, the linear model used to generate residuals, the estimated heritability (with standard error and p-value) and which category the phenotype belongs to. The covariates used in the linear models are described at the bottom of the main table

Supplementary Table 2: List of variants

Number of SNPs called on each chromosome: The total number of SNPs is split according to position relative to protein coding genes: Non-coding, splice region, synonymous, non-synonymous and STOP loss/gain. We report the number of number of variants predicted to be deleterious (SIFT) or cause nonsense mediated decay. The number of protein coding genes affected by the different categories appears at the bottom of the table.

Supplementary Table 3: Number of variants during the discovery and imputation process.

The number of known and novel SNPs detected during the process from raw variant calling through to post imputation following quality control (QC). Ti/Tv ratios are given for each tranche of SNPs. The table also reports the number of SNPs that passed imputation QC after annotation with the latest release of the Mouse Genomes Project (2016 release REL-1505). VQSR = variant quality score recalibration, MGP = Mouse Genomes Project.

Supplementary Table 4: SNPs occurring in Inbred Strains

For the 5.7M SNPs used for mapping, report the number, cumulative total and cumulative fraction of sites observed to be polymorphic in 38 inbred strains in the Sanger Mouse Genomes database version 1505. The strains are arranged so that wild-derived strains are last. A SNP is assigned to a strain only if no preceding strain in the table carries the non-reference (alternate) allele.

Supplementary Table 5: List of 255 detected QTLs (FDR<5%)

We report the position (chr:bp) of the strongest associated SNP at each QTL with –logP value, minor allele frequency, FDR , variance explained and beta. Also reported is the 95% Confidence Interval (start,-finish) with the number and names of protein

coding genes present inside the interval. If the 95% CI doesn't include any coding gene we report the 2 closest neighbouring genes (5' and 3' direction, respectively).

Supplementary Table 6: List of 156 unique QTLs

Here we report the 156 unique QTLs and candidate genes. Additional phenotypes mapping on the same QTL are also listed. References point to literature supporting suggested candidate genes. * means the candidate gene reported lies outside the 95% CI zone. The last column indicates if a knock-out exist supporting the candidate gene effect.

Supplementary Table 7: Power to detect QTLs

Power to detect QTLs in the CFW population as a function of genome-wide significance (sig, with corresponding logP threshold), sample size N, QTL and effect size V (fraction of variance explained by QTL). Lines with grey indicate power for the median sample size (1732) and effect size (0.016) in the current study.

Supplementary Methods

Phenotyping

Behavior

Anxiety was modeled by 3 tests: Five minutes activity in a bright lit round arena (Open Field Test), Elevated Plus Maze and latency to eat a novel food after 10 hours food restriction (Neophagia). We also measured home cage activity over a 30 minutes period using photoactivity system from San Diego Instruments (San Diego, CA). Protocols for these tests have been described in [1]. Pre-pulse inhibition of startle (Startle PPI) was measured and analyzed as previously described, using 3 different pulse and 3 different prepulse intensities [2,3]. Fear conditioning was performed following the protocol in [4], keeping the order of context and cue testing sessions identical for all mice. On the first day of the test mice were subjected to a 13 minutes training session during which they were placed in a Perspex enclosure with a metal grid floor and received 2 electric foot shocks (0.3mA, 0.5sec) preceded by a 30 seconds tone. In the morning of the second day of the test the mice were placed in the same enclosure for 5 minutes and fear associated with the context was measured by the amount of freezing. In the afternoon the animals were placed in a different enclosure for 5 minutes where they were subjected to two 30 seconds tones without any paired electric shock. The fear associated to the cue was assessed by measuring the freezing behaviour during tones. Freezing behaviour during all sessions of the test was scored using a VideoTrack automated system (Viewpoint, Champagne Au Mont D'Or, France). Because the distribution of the measures varied

significantly between the 4 enclosures in which the mice where tested for fear conditioning, we quantile normalised the data per enclosure before performing further analysis. Depressive-like behavior of mice was assessed with the forced swim test [5]. Animals were placed for 6 minutes in a 30cm diameter plastic cylinder filed with water at 25°C. Immobility of the mice during the last 4 minutes was scored using VideoTrack FST automated system (Viewpoint, Champagne Au Mont D'Or, France).

Ventilatory responses to acute hypoxia

Ventilatory responses to acute hypoxia were measured using whole body plethysmography. Awake unrestrained mice were placed in individual plethysmographs (550 ml volume, Model PLY3211, Buxco, Wilmington, NC USA) to which premixed gases were delivered at a rate of 2 L min^{-1}. After a brief (5-min) acclimatisation period, mice were exposed to 15 min of 21% O_2, balance N_2 (pre-normoxia), followed by 5 min of 10% O2, balance N_2 (hypoxia), followed by a final 5-min period of 21% O_2 (post-normoxia). Tidal volume (TV) and respiratory frequency (f) were measured continuously, and used to calculate minute ventilation (MV). For each of these three parameters, the following indices of the respiratory phenotype were derived: *i)* Baseline (mean value for MV, TV or *f* during the final 3 min of pre-normoxia); *ii)* Acute Hypoxic Response (AHR, difference between the mean value during first 30 sec of hypoxia and the Baseline); *iii)* Hypoxic Ventilatory Decline (HVD, difference between mean value during the first 30 sec of hypoxia and mean value during final 2 min of hypoxia); *iv)* Undershoot (difference between

mean value during the first 30 sec of post-normoxia and the Baseline); *v)* Off-Response (difference between mean value during first 30 sec of post-normoxia and mean value during final 2 min of hypoxia); *vi)* Sustained Hypoxia Response (SHR, difference between Off-Response and Undershoot); and *vii)* Normoxic Recovery (NR, difference between value during first 30 sec of post-normoxia and final 2 min of post-normoxia).

Electrocardiography

For surface electrocardiography (ECG), mice were anesthetized using isoflurane inhalation (induction: 4.0 volume % in oxygen; maintenance: 1.5-2.5 volume %). Surface ECGs were recorded from subcutaneous 23-gauge needle electrodes attached to each limb using the Powerlab acquisition system (ADInstruments). ECG traces were signal averaged and analysed for heart rate (RR interval), PRmain (interval between start P wave and start QRS complex), PRpeak (interval between start P wave and R peak), QRSmain (interval between start of QRS complex and S peak), QRSpeak (interval between R peak and S peak), QTmain (interval between start of QRS complex and end of T wave), and QTpeak (interval between R peak and end of T wave) using the LabChart7Pro software (ADInstruments). QTmain and QTpeak intervals were corrected for heart rate using the formula: $QTc=QT/(RR/100)^{1/2}$ (RR in ms).

Sleep

At the end of the phenotyping pipeline mice were moved to individual cages to assess their baseline sleeping behaviour using a non-invasive EEG-validated piezo-

electric sleep recording system [6] (MouseRec system by Signal Solutions, LLC, Lexington, KY, USA). Sleep was recorded for 72 hours but only the last 48 hours were used for analysis thus allowing one day of habituation. Light-dark cycle (12h:12h light:dark) and ambient temperature (21°C) during the recordings were the same as in the colony rooms. In each of the 1607 mice for which good quality signals could be obtained, 19 sleep phenotypes were quantified concerning the amount of sleep, its distribution over the 24h day, and the fine structure of sleep (e.g. sleep bout duration and sleep fragmentation). All values are reported per 24h and represent the average over the last two 24h recording periods starting at light onset.

Body weight

We measured body weight at 17, 18, 19 and 20 weeks of age. The last measure was collected immediately before sacrifice after overnight fast. We calculated Body Mass Index (BMI) by dividing the body weight at 20 weeks by the square of the body length, collected at the same time. We also calculated a "pseudo BMI" dividing the body weight at 20 weeks by the square of the length of the tibia.

At 20 weeks of age mice were sacrificed between 8am and 12pm after overnight food restriction and tissues harvested for further measures. We measured body and tail length during the procedure.

Haematology

Whole blood samples for haematology were collected by cardiac puncture into 200µl EDTA coated paediatric tubes. Samples were placed on a rotary mixer for 30 minutes before full blood count and differential analyses were performed on board a Siemens Advia 2120 haematology analyser.

Clinical Chemistry

Blood samples were collected by cardiac puncture into 1ml lithium heparin-coated paediatric tubes. Samples were mixed by gentle inversion and centrifuged within 2 hours of collection at 5000 X g, for 10 minutes in a refrigerated centrifuge set at 8°C. 200µl of plasma was collected from each sample and analysed on board a Beckman Coulter AU680 clinical chemistry analyser using reagents and settings as recommended by the manufacturer for the following profile of 20 tests: sodium, potassium, chloride, urea, creatinine, total calcium, inorganic phosphorous, alkaline phosphatase (ALP), alanine aminotransferase (ALT), aspartate aminotransferase (AST), lactate hedydrogenase (LDH), total protein, albumin, total cholesterol, HDL cholesterol, LDL cholesterol, glucose, triglycerides, glycerol, free fatty acids, total bilirubin, iron and alpha amylase.

Platelet serotonin

A small aliquot of whole blood was immediately snap frozen after collection by cardiac puncture into a lithium heparin-coated tube. At the time of measure 10µl of this whole blood aliquot was thawed and used for serotonin quantification.

Serotonin was extracted by adding 390 µl of 10-3 M HCl containing sodium metabisulfite, EDTA and ascorbic acid. After 30 sec shaking, samples were centrifuged at 20000g for 20 min at 5°C. The supernatants were collected and filtered through a 10 kDa membrane (Nanosep, Pall) by centrifugation at 7000g. Then, a 20 µl aliquot was analysed for serotonin by fluorometric detection [7].

Micronucleus

We measured the formation of micronuclei, markers of genomic stability, in erythrocytes by flow cytometry [8].

Neurogenesis

Following sacrifice the brain was weighted and then split in two halves by sagittal section and the left hemisphere fixed overnight in 4% paraformaldehyde followed by dehydration in 30% sucrose solution for 3-5 days. Sections (40 µm) were prepared on a freezing microtome and stored in antifreeze solution at −20°C. We measured hippocampal neurogenesis by Ki67 and DCX staining [9], counting labelled cells on every sixteenth (DCX) or eighth (Ki67) section through the entire rostrocaudal extent of the granule cell layer.

Wound healing

We measured healing of hole punctures made to the animal's ears following the approach described in [10]. A 2-mm diameter hole was made in the center of each ear when the mice started the phenotyping pipeline (16 weeks old) and following sacrifice 5 weeks later ears were fixed and stored in 4% paraformaldehyde. Both

ears were then flattened between 2 coverslips, scanned at 600dpi and the image analysed with the ImageJ software to measure the area of the hole still open. We excluded ears when the hole merged with the edge of the ear and only analysed mice when both ear measures were available.

Adrenal weight

Following sacrifice adrenals were removed together with the kidneys, fixed and stored in 4% paraformaldehyde. Adrenals were dissected from the kidneys at a later day and their weight measured. Data was analysed only when weight from both adrenals was available.

Immunology

Following sacrifice, mouse spleens were stored in PBS on ice prior to processing. Splenocytes were extracted by mashing the spleen through a 45µm filter using the plunger end of a syringe. The cells were then washed extensively with PBS and re-filtered prior to staining. Erythrocyte contamination in the splenocyte sample was minimal. Splenocytes were stained with fixable near-IR dead cell stain (Life Technologies), CD3e PE Cy7, CD45 V450, CD44 FITC, CD4 V500 (all BD Bioscience), CD49b APC, CD19 PE, CD8a PerCP Cy5.5 (all eBioscience) for 25 minutes in the dark at 4°C before being fixed in 2% formaldehyde solution. Data were collected using a 3-laser LSRII or MACSQuant flow cytometer and analysed on Flowjo v8.4 (Treestar, OR, USA).

Muscle weight and tibia length

Following sacrifice, one hindlimb was removed and transferred to a -70 °C freezer. On the day of dissection, the leg was defrosted and two dorsiflexors (tibialis anterior (TA), and extensor digitorum longus (EDL)), and three plantar flexors (gastrocnemius ("gastroc"), plantaris and soleus) were dissected under a microscope. Each muscle was weighed to a precision of 0.1 mg on a balance (Pioneer, Ohaus). A panel of muscles was examined because muscles of different size, shape, proportion of the oxidative and glycolytic fibres, or pattern of activation may be affected by different genetic mechanisms. The soft tissues were removed from the tibia and bone length was measured to a precision of 0.01 mm with a digital caliper (Z22855, OWIM GmbH & Co).

Apparent bone mineral content

Mineral content of the tibia was measured with the Faxitron MX-20 scanner (Faxitron Bioptics LLC, AZ, USA) using methods adapted from (Bassett *et al.,* 2012). Three types of materials; 0.8 mm of aluminium, 1.0 mm of polystyrene and 0.8 mm of steel, were scanned together with the bones for calibration of the image. ImageJ (V1.48p, National Institutes of Health, USA) was used to quantify the apparent bone mineral content, appBMC, and the bone size. The appBMC was characterized by the mean, mode, median, minimum, maximum, standard deviation, skewness and kurtosis of the optical density of bone image. The bone area, perimeter, Feret's diameter (longest distance between 2 points on the perimeter), and width and height of the bounding rectangle characterized the bone size.

References

1. Solberg, L.C. *et al.* A protocol for high-throughput phenotyping, suitable for quantitative trait analysis in mice. *Mamm Genome* **17**, 129-46 (2006).
2. Yee, B.K., Chang, T., Pietropaolo, S. & Feldon, J. The expression of prepulse inhibition of the acoustic startle reflex as a function of three pulse stimulus intensities, three prepulse stimulus intensities, and three levels of startle responsiveness in C57BL6/J mice. *Behav Brain Res* **163**, 265-76 (2005).
3. Yee, B.K. & Feldon, J. Distinct forms of prepulse inhibition disruption distinguishable by the associated changes in prepulse-elicited reaction. *Behav Brain Res* **204**, 387-95 (2009).
4. Line, S.J. *et al.* Reduced sensitivity to both positive and negative reinforcement in mice over-expressing the 5-hydroxytryptamine transporter. *Eur J Neurosci* **40**, 3735-45 (2014).
5. Porsolt, R.D., Le Pichon, M. & Jalfre, M. Depression: a new animal model sensitive to antidepressant treatments. *Nature* **266**, 730-2 (1977).
6. Mang, G.M. *et al.* Evaluation of a piezoelectric system as an alternative to electroencephalogram/ electromyogram recordings in mouse sleep studies. *Sleep* **37**, 1383-92 (2014).
7. Kema, I.P. *et al.* High performance liquid chromatographic profiling of tryptophan and related indoles in body fluids and tissues of carcinoid patients. *Clin Chim Acta* **221**, 143-58 (1993).
8. Balmus, G. *et al.* A high-throughput in vivo micronucleus assay for genome instability screening in mice. *Nat Protoc* **10**, 205-15 (2015).
9. Huang, G.J. *et al.* A genetic and functional relationship between T cells and cellular proliferation in the adult hippocampus. *PLoS Biol* **8**, e1000561 (2010).
10. Clark, L.D., Clark, R.K. & Heber-Katz, E. A new murine model for mammalian wound repair and regeneration. *Clin Immunol Immunopathol* **88**, 35-45 (1998).

Supplementary Table 2

Chr	All	Non-coding	Splice region	Synonymous	Splice site	Non-synonymous	Nonsense-mediated decay	Deleterious (SIFT)	STOP loss / gain
1	532,059	528,561	292	2,037	4	946	66	149	2 / 2
2	486,234	481,561	335	2,650	13	1,215	263	189	2 / 6
3	287,515	286,055	103	823	4	428	55	46	0 / 1
4	265,571	262,063	285	1,774	4	817	503	109	3 / 13
5	276,276	274,106	206	1,359	4	518	21	60	1 / 1
6	450,874	447,769	278	1,592	11	968	79	163	4 / 10
7	183,664	180,559	198	1,561	4	929	242	160	1 / 10
8	219,205	217,411	147	1,097	3	476	-	68	0 / 3
9	263,913	261,922	148	1,193	3	488	81	72	3 / 3
10	207,149	205,708	136	907	-	359	-	37	1 / 1
11	392,904	388,863	332	2,446	5	1,047	57	144	1 / 9
12	415,846	413,586	219	1,306	6	636	-	88	1 / 4
13	356,388	354,200	161	1,279	1	514	154	75	0 / 4
14	480,158	478,908	91	782	2	327	-	47	0 / 1
15	233,652	232,172	149	900	4	353	19	55	0 / 0
16	51,279	50,947	22	180	1	124	-	5	0 / 0
17	321,736	317,877	303	2,079	2	1,084	197	181	1 / 12
18	174,311	172,839	89	913	1	412	-	56	0 / 1
19	121,541	120,513	93	676	2	226	-	29	0 / 2
X	46,553	46,339	16	115	1	64	-	17	0 / 1
Total	**5,766,828**	**5,721,959**	**3,603**	**25,669**	**75**	**11,931**	**1,737**	**1,750**	20 / 84
Protein coding	9,141	-	361	3,424	39	3,938	38	1,242	19 / 80

Genes

Supplementary Table 4

strain	#additional snps	cumulative #snps	fraction.accounted
FVB_NJ	2187997	2187997	0.3794
A_J	835752	3023749	0.5243
AKR_J	584264	3608013	0.6256
BALB_cJ	128890	3736903	0.6480
CBA_J	180544	3917447	0.6793
C3H_HeJ	21234	3938681	0.6830
DBA_2J	168095	4106776	0.7121
LP_J	272355	4379131	0.7594
BUB_BnJ	188913	4568044	0.7921
129P2_OlaHsd	31993	4600037	0.7977
129S1_SvImJ	703	4600740	0.7978
129S5SvEvBrd	802	4601542	0.7979
BTBR_T+_Itpr3tf_J	52511	4654053	0.8070
C3H_HeH	534	4654587	0.8071
C57BL_10J	3011	4657598	0.8077
C57BL_6NJ	7	4657605	0.8077
C57BR_cdJ	40496	4698101	0.8147
C57L_J	5392	4703493	0.8156
C58_J	31001	4734494	0.8210
DBA_1J	3118	4737612	0.8215
I_LnJ	73656	4811268	0.8343
KK_HiJ	128623	4939891	0.8566
NOD_ShiLtJ	156125	5096016	0.8837
NZB_B1NJ	56233	5152249	0.8934
NZO_HlLtJ	50330	5202579	0.9022
NZW_LacJ	27409	5229988	0.9069
RF_J	20130	5250118	0.9104
SEA_GnJ	7200	5257318	0.9116
ST_bJ	23959	5281277	0.9158
LEWES_EiJ	68912	5350189	0.9278
ZALENDE_EiJ	83913	5434102	0.9423
WSB_EiJ	20537	5454639	0.9459
CAST_EiJ	75149	5529788	0.9589
MOLF_EiJ	52117	5581905	0.9679
PWK_PhJ	16509	5598414	0.9708
SPRET_EiJ	15743	5614157	0.9735

Supplementary Table 6

Phenotype	Chr	Position (Mb)	-logP	Additional phenotypes mapping at the same locus	-logP of add. phenotypes (range)	Nb of genes under QTL (95% CI)	Candidate gene(s) under QTL	Findings supporting candidate genes	KO?
Bioch.CreatinineEnzymatic	1	20.5	5.0			15	*Pkhd1*	Mutations in humans cause autosomal recessive polycystic kidney disease (1)	X
PAS.Total_Activity	1	51.6	5.4			5	*Gls*	Regulates glutamate level in the brain (2)	X
Tibia.Length	1	86	4.5			12	*Gpr55*	Affects osteoclast function in vitro and bone mass in vivo (3)	X
FC.Context.Freeze.Corrected	1	105.9	6.7			7	*Phlpp1*	Involved in hippocampus memory formation (4)	X
Neuro.DCX	1	135.3	8.4			8			
BMC.StdDev	1	151.2	6.6	BMC.StdDev.N	5.63	15			
Muscles.EDL.g	1	151.9	5.3			7			
Haem.RDW	1	153.3	5.5			28			
Haem.MCV	1	155.7	5.6			3			
FACS.CD45posCD3negDX5pos	1	168.1	4.7			1			
Bioch.Tot.Cholesterol	1	171.4	9.2	Bioch.HDL	8.36	26	*Apoa2*	Mutant mice show decrease HDL and total cholesterol levels (5)	X
FACS.CD3posCD8pos	1	173.9	5.0			4			
Neuro.Ki67	1	177.6	6.8			14			

FACS.CD45posCD3negDX5pos	2	28.9	5.2			19			
Micronucleus.Mn.NCE	2	30	5.2			20			
FACS.CD45posCD3negDX5pos	2	44.4	4.7			2	*Zeb2*	Essential for terminal NK cell maturation and homeostasis of the NK cell pool (6)	
Cardio.ECG.PR_main	2	91.5	5.6			195			
FACS.CD3posCD44posCD4CD8Ratio	2	102.7	11.7	FACS.CD3posCD8posCD44pos	8.77	2	*Cd44*	Protein directly involved in the phenotype (7)	X
WH.Ears_Area	2	134.1	5.5			1	*Bmp2*	Promotes cartilage formation (8)	
Hypoxia.f_HVD	2	152	5.8			14			
EPM.ClosedArms.Entries	2	153.7	5.8			14			
Muscles.Sol.g	2	155.4	7.1	Muscles.TA.g, Muscles.EDL.g, Muscles.Plant.g	4.53-6.39	33			
BMC.Width	2	155.6	4.8			33			
Haem.EOS_percent	2	163.8	5.2			14			
Muscles.Sol.g	3	14.8	7.2			9	*Car3*	Abundant in skeletal muscle. Mutants muscles have shorter relaxation half times (9)	X
Muscles.Gast.g	3	19.1	5.3			4			
Haem.LYM_percent	3	20	6.6			9			
FACS.CD45posCD3negDX5pos	3	116.2	5.1			17			
FACS.CD45posCD3negCD19pos	4	97.8	5.0			9			
Bioch.CreatinineEnzymatic	4	100.9	5.4			12			
EPM.Total.Distance	4	117.4	4.9			23			
FACS.CD3posCD44posCD4CD8Ratio	4	134.2	5.8			17	*Cd52*	Regulates T cells by interacting with the inhibitory receptor Siglec-10 (10)	
Tibia.Length	4	134.6	4.9			55	*Hspg2*	Mutant mice long bones	X

								approximately half of the size of wild-types (11)	
Bioch.ALP	4	137.7	133.7			2	*Alpl*	Protein directly involved in the phenotype (12)	X
FACS.CD3posCD4CD8Ratio	4	149.9	4.6			13	*Tnfrsf9*	Influences T cell response (13)	X
BMC.Mean	5	24.4	8.3	BMC.StdDev, BMC.StdDev.N, BMC.Max.N, BMC.Median, BMC.Kurt, BMC.Max, BMC.Kurt.N	7.65-12.62	16	*Slc4a2*	Deletion in mice results in osteopetrosis (14)	X
Tibia.Length	5	40.7	4.8	BMC.Width	4.49	3	*Nkx3-2*	Negative regulator of chondrocyte maturation (15). Null mice are affected by a perinatal lethal skeletal dysplasia (16)	X
EPM.Total.Distance	5	50.6	5.2	EPM.ClosedArms.Distance	4.88	2	*Adgra3*	Specifically expressed in the choroid plexus and is upregulated following brain injury (17)	
Tibia.Length	5	51.7	4.5			1			
Sleep.long_sleep	5	51.8	6.8			1	*Ppargc1a*	Stimulates the expression of clock genes (18)	
PAS.Total_Activity	5	119.7	4.9			3			
Bioch.Tot.Cholesterol	5	125.1	18.5	Bioch.LDL, Bioch.HDL	16.1-20.04	6	*Scarb1*	Abnormal lipoprotein metabolism in deficient mice (19)	X
Haem.measHGB	5	148.1	6.4	Haem.CHCM	6.3	3	*Slc7a1*	Peripheral blood from mutant mice contains 50% fewer red blood cells and reduced hemoglobin levels (20)	X

Micronucleus.Mn.NCE	5	148.8	4.7			3			
BMC.Width	6	15.1	4.2			3			
Muscles.Sol.g	6	17.5	16.2	Muscles.TA.g, Muscles.Plant.g, Muscles.EDL.g, Muscles.Gast.g	7.46-9.94	1	*Met*	Essential for muscle formation (21) and regeneration (22)	X
SPPI.ln_pa	6	17.5	6.7			1			
Bioch.Calcium	6	17.5	8.3			1			
Bioch.Tot.Cholesterol	6	17.5	6.1			1			
Bioch.Tot.Protein	6	17.5	27.7	Bioch.Albumin	25.8	1			
FACS.CD3posCD4CD8Ratio	6	41.1	7.9	FACS.CD3posCD8pos, FACS.CD3posCD4pos	7.73-8.49	8			
Haem.PDW	6	78.2	6.1			0			
EPM.Total.Distance	6	110.2	5.6			1	*Grm7*	Mutant mice more active in the initial minutes following placement in a novel environment (23)	X
Muscles.Plant.g	6	112.3	4.7			37			
Bioch.LDH	6	123.9	15.4			21			
Tibia.Length	6	147	10.9	BMC.Width, BMC.Perim	6.03-10.47	3	*Arntl2*	Interacts with HIF-2alpha during skeletal growth and osteoarthritis development (24)	
FACS.CD45posCD3negCD19pos	7	72.2	6.2			1			
BMC.Width	7	79.2	4.6			6			
Micronucleus.Mn.NCE	8	33.2	13.1			13	*Wrn*	Resolves aberrant DNA structures arising from DNA metabolic processes (25, 26)	X
Cardio.ECG.PR_main	8	80.3	6.0			10			
Haem.MCV	8	81.2	5.4			6	*Gypa*	Major intrinsic membrane	

								sialoglycoprotein of the erythrocyte, required for the expression of O-linked antigens on the cell membrane (27)	
FACS.CD3posCD4CD8Ratio	8	82.4	8.7	FACS.CD3posCD44negCD4CD8Ratio, FACS.CD3posCD8pos, FACS.CD3posCD4pos	6.96-9.48	1	*Il15*	T cell growth factor (28)	X
WH.Ears_Area	8	116.1	6.7			0	*Maf (213,880bp distant from 95% CI)*	Expressed in hypertrophic chondrocytes (29, 30)	X
FACS.CD45posCD3negCD19pos	9	32.5	5.8			1	*Fli1*	Modulates B cell development (31)	X
Sleep.long_sleep	9	73.8	5.5			1			
Tibia.Length	9	81.2	8.7	BMC.Width	5.55	8	*Htr1b*	Mediates serotonin effect on osteoblasts proliferation (32)	X
OFT.Arena.Distance	9	81.2	5.3	OFT.Periphery.Distance	5.67	12	*Htr1b*	Knockout mice show reduced anxiety (33)	X
Muscles.Sol.g	9	87.8	5.6			13			
Muscles.Plant.g	9	89.5	6.6			14			
Micronucleus.Mn.NCE	9	109.1	5.4			20	*Trex1*	3’-5’ DNA exonuclease. Mutants recapitulate the phenotype (34)	X
SPPI.pReactivity	10	57.8	7.1			3	*Fabp7*	Fabp7-deficient mice show decreased PPI and a shortened startle response latency (35)	X

SPPI.pc_average_ABC	10	66.8	6.3	SPPI.ppReactivity, SPPI.slpPPI_average, SPPI.pc_average_pA	5.31-6.61	0			
SPPI.pReactivity	10	68	8.0			1			
Muscles.Plant.g	10	84.3	4.8			9			
Micronucleus.Mn.NCE	10	121.5	8.6			6	*Rassf3*	Member of the RASSF family of proteins that function as tumor suppressors (36)	
EPM.Total.Distance	11	7	4.7			0	*Adcy1 (62,068bp distant from 95% CI)*	Mice overexpressing Adcy1 in the forebrain exhibit hyperactive behaviors (37)	X
Muscles.TA.g	11	17.6	6.3			1			
EPM.Total.Distance	11	19.7	5.9	EPM.ClosedArms.Distance	5.94	15			
OFT.Arena.Distance	11	25.7	6.7	OFT.Periphery.Distance, OFT.Open.Distance, EPM.Total.Distance	5.53-6.22	2			
PAS.Total_Activity	11	28.1	5.5			2			
Haem.HDW	11	32.2	6.0			20			
Tibia.Length	11	33.4	4.1			25			
Sleep.long_sleep	11	38.4	4.9	Sleep.short_sleep, Sleep.Ampl	5.69-6.07	3			
Hypoxia.f_HVD	11	38.8	7.7	Hypoxia.f_Undershoot, Hypoxia.f_SHR, Hypoxia.MV_HVD	5.62-7.21	5			
FACS.CD45posCD3negCD19pos	11	44.4	5.5			4	*Ebf1*	Plays a specific and important role in the transcriptional control of B-cell differentiation (38)	X

Haem.abs_eos	11	44.6	5.4			0			
Micronucleus.Mn.NCE	11	69.6	8.2			49	*Trp53, Aurkb*	Trp53 is an important tumor suppressor (39) and Aurkb plays a crucial role in cell cycle control and mitosis (40)	
Weight.Diss	11	83.8	4.9			32			
Muscles.TA.g	11	90.2	6.0	Muscles.Gast.g	5.78	10			
Muscles.TA.g	11	96.1	4.9			45			
Tibia.Length	11	96.5	4.6	BMC.Width, BMC.Perim	5.61-6.21	54			
Haem.HDW	11	96.8	17.4	Haem.RDW, Haem.PLT, Haem.PCT	8.04-12	32	*Nfe2l1*	Homozygous mutant mice are anemic due to a non-cell autonomous defect in definitive erythropoiesis (41)	X
Hypoxia.f_SHR	11	96.8	7.2	Hypoxia.TV_Undershoot	6.15	33			
PAS.Last10	11	96.8	5.4			78			
BMC.Mean	11	96.9	24.9	BMC.Kurt.N, BMC.Max.N, BMC.Max, BMC.Kurt, BMC.StdDev, BMC.StdDev.N, BMC.Mean.N, BMC.Median, BMC.Median.N, BMC.Mode, BMC.Mode.N	6.28-29.36	24			
FACS.CD3posCD4posCD44pos	11	97.1	8.6	FACS.CD3posCD8posCD44pos	6.21	15	*Tbx21*	Regulates T cell homeostasis and function (42, 43)	X
Muscles.Plant.g	11	98.2	4.5			41			
FACS.CD45posCD3negCD19pos	11	98.4	6.9	FACS.CD45posCD3posCD4pos, FACS.CD3pos	5.89-6.1	41			
FACS.CD45posCD3negDX5pos	11	99	6.4			78			
BMC.Median	11	108.2	4.6			1	*Prkca*	Age-related bony invasion of	X

								the medullary cavity at specific sites of the long bones in mutant mice (44)	
Bioch.Tot.Protein	11	110.1	5.5			2			
FACS.CD3posCD8pos	12	25.5	5.4	FACS.CD45posCD3posCD8pos, FACS.CD3posCD4CD8Ratio, FACS.CD3posCD44negCD4CD8Ratio, FACS.CD3posCD8posCD44pos	5.16-7.32	1	*Id2*	Mediates CD8+ T cell immunity (45)	X
Cardio.ECG.QRS_peak	12	80.5	6.1			11	*Actn1*	Cytoskeletal protein of the cardiomyocyte (46)	
Muscles.TA.g	12	83.5	5.4			6	*Dpf3*	Regulates muscle development (47)	
Tibia.Length	12	83.6	7.1	BMC.Width, BMC.Perim	5.54-7.22	1			
Muscles.EDL.g	12	83.8	5.8			17			
Tibia.Length	12	91.3	8.9	BMC.Width	6.19	5	*Tshr*	Femur length and weight are reduced in null mice (48)	X
PAS.Last10	13	7.3	10.6	PAS.Total_Activity	8.51	1	*Adarb2*		
Weight.Diss	13	10.6	4.9			10	*Chrm3, Wdr37*	Chrm3 (49) and Wdr37 (34) mutants show decreased body weight	X
Muscles.Sol.g	13	16.3	5.9			3			
Tibia.Length	13	110.5	4.3			4			
Muscles.Sol.g	13	114.4	13.0			10	*Fst*	Promotes muscle growth (50, 51)	X
Muscles.Plant.g	13	117.3	5.9			3			
Hypoxia.f_HVD	13	117.9	5.9			1			
Muscles.TA.g	14	25.6	5.0			26			

EPM.Total.Distance	14	82.1	6.2			1	*Pcdh17*	Deficiency in mice affects synaptic transmission and decreases depression-like phenotypes (52)	X
Haem.MCV	14	96.2	5.0			8			
Bioch.Amylase	15	7.5	7.1			2	*Gdnf*	Required for neural colonization of the pancreas (53)	X
Tibia.Length	15	11.7	9.1	BMC.Width, BMC.Perim	5.36-11.01	7	*Nprs3*	Null mice exhibit striking skeletal abnormalities, including elongated tibia length, due to increased bone turnover (54)	X
BMC.Width	15	26.6	5.3			1			
BMC.Width	15	33.8	4.3			42			
BMC.Median	15	86.5	5.7			13	*Wnt7b*	Promotes bone formation (55, 56)	X
BMC.Max	17	9.3	4.6			0			
OFT.Open.Distance	17	24.8	5.5			48			
Haem.MCV	17	30.9	6.3			38	*Pim1*	Null mice have abnormally small erythrocytes (57)	X
FACS.CD3posCD8pos	17	34	77.0	FACS.CD3posCD44posCD4CD8Ratio, FACS.CD3pos, FACS.CD3posCD4pos, FACS.CD3posCD4CD8Ratio, FACS.CD3posCD44negCD4CD8Ratio, FACS.CD45posCD3negDX5pos, FACS.CD45posCD3posCD8p	6.56-69.62	57			

				os, FACS.CD3posCD4posCD44pos					
Weight.Diss	17	34.1	5.3			104			
Micronucleus.Mn.NCE	17	34.2	9.3			86			
Haem.HDW	17	34.8	7.9			72			
Cardio.ECG.Heart_Rate	17	35.3	7.9			106			
Bioch.ALAT	17	36.1	5.6			160			
Haem.CHCM	17	36.1	5.1			106			
FACS.CD3posCD44negCD4CD8Ratio	17	43.4	10.4	FACS.CD3posCD4pos, FACS.CD3posCD8pos, FACS.CD3posCD4CD8Ratio	5.64-9.72	21			
Haem.RBC	17	48.4	5.4	Haem.MCV	5	17			
BMC.Median	17	49.7	5.0			6	*Daam2*	Mutant mice show decreased bone mineral content (34)	X
Haem.EOS_percent	17	70.4	5.2			1			
Adrenals.Adrenals_g	17	74.5	7.7			9			
Muscles.Plant.g	17	85.2	5.1			3	*Camkmt*	Muscles strength reduced in mutants (58)	X
BMC.Mean	18	38.4	7.0	BMC.StdDev.N, BMC.StdDev, BMC.Median, BMC.Mean.N	5.94-7.01	8	*Spry4*	Null mice show severe defects in limb morphogenesis (59)	X
FACS.CD3posCD4CD8Ratio	18	69.9	4.5			3	*Tcf4*	Deficiency leads to a partial block in both B and T lymphocyte development in the mouse (60)	X
FACS.CD3posCD4pos	19	22	6.0			4			
Muscles.TA.g	19	25.7	4.9			3	*Dmrt2*	Regulates myogenic determination gene MYF5 (61)	X
BMC.Width	19	26.9	4.3			5			

Weight.Diss	X	85.1	4.5			4			
Tibia.Length	X	97.5	5.8			7			
Muscles.EDL.g	X	99.5	6.5			12			
Weight.Startle	X	106.1	8.3	Weight.Average, Muscles.Sol.g, Weight.Diss	5.83-7.88	12			
Weight.Hypo	X	106.2	7.0			12			
BMC.Max.N	X	106.4	6.5	BMC.Max	5.36	13	*Cysltr1*	Involved in 5-Lipoxygenase mediated osteoclastogenesis (62)	
Muscles.Gast.g	X	109.6	19.4	Muscles.EDL.g, Muscles.TA.g, Muscles.Plant.g	7.32-29.1	3			
Diss.Brain.Weight	X	109.6	9.8			3			
BMC.Area	X	109.7	10.7			7			
Bioch.CreatinineEnzymatic	X	109.7	6.5			3			
BMC.StdDev	X	110.6	6.8	BMC.StdDev.N	5.77	5			
Haem.EOS_percent	X	155.6	6.0			1			
PAS.Total_Activity	X	156.7	5.7			7			

References

1. Bakeberg JL, Tammachote R, Woollard JR, Hogan MC, Tuan HF, Li M, et al. Epitope-tagged Pkhd1 tracks the processing, secretion, and localization of fibrocystin. J Am Soc Nephrol. 2011;22(12):2266-77.
2. El Hage M, Masson J, Conjard-Duplany A, Ferrier B, Baverel G, Martin G. Brain slices from glutaminase-deficient mice metabolize less glutamine: a cellular metabolomic study with carbon 13 NMR. J Cereb Blood Flow Metab. 2012;32(5):816-24.
3. Whyte LS, Ryberg E, Sims NA, Ridge SA, Mackie K, Greasley PJ, et al. The putative cannabinoid receptor GPR55 affects osteoclast function in vitro and bone mass in vivo. Proc Natl Acad Sci U S A. 2009;106(38):16511-6.
4. Shimizu K, Phan T, Mansuy IM, Storm DR. Proteolytic degradation of SCOP in the hippocampus contributes to activation of MAP kinase and memory. Cell. 2007;128(6):1219-29.

5. Weng W, Breslow JL. Dramatically decreased high density lipoprotein cholesterol, increased remnant clearance, and insulin hypersensitivity in apolipoprotein A-II knockout mice suggest a complex role for apolipoprotein A-II in atherosclerosis susceptibility. Proc Natl Acad Sci U S A. 1996;93(25):14788-94.
6. Eberl G, Di Santo JP, Vivier E. The brave new world of innate lymphoid cells. Nat Immunol. 2015;16(1):1-5.
7. Stoop R, Kotani H, McNeish JD, Otterness IG, Mikecz K. Increased resistance to collagen-induced arthritis in CD44-deficient DBA/1 mice. Arthritis Rheum. 2001;44(12):2922-31.
8. Duprez DM, Coltey M, Amthor H, Brickell PM, Tickle C. Bone morphogenetic protein-2 (BMP-2) inhibits muscle development and promotes cartilage formation in chick limb bud cultures. Dev Biol. 1996;174(2):448-52.
9. Kim G, Lee TH, Wetzel P, Geers C, Robinson MA, Myers TG, et al. Carbonic anhydrase III is not required in the mouse for normal growth, development, and life span. Mol Cell Biol. 2004;24(22):9942-7.
10. Bandala-Sanchez E, Zhang Y, Reinwald S, Dromey JA, Lee BH, Qian J, et al. T cell regulation mediated by interaction of soluble CD52 with the inhibitory receptor Siglec-10. Nat Immunol. 2013;14(7):741-8.
11. Costell M, Gustafsson E, Aszodi A, Morgelin M, Bloch W, Hunziker E, et al. Perlecan maintains the integrity of cartilage and some basement membranes. J Cell Biol. 1999;147(5):1109-22.
12. Narisawa S, Frohlander N, Millan JL. Inactivation of two mouse alkaline phosphatase genes and establishment of a model of infantile hypophosphatasia. Dev Dyn. 1997;208(3):432-46.
13. DeBenedette MA, Wen T, Bachmann MF, Ohashi PS, Barber BH, Stocking KL, et al. Analysis of 4-1BB ligand (4-1BBL)-deficient mice and of mice lacking both 4-1BBL and CD28 reveals a role for 4-1BBL in skin allograft rejection and in the cytotoxic T cell response to influenza virus. J Immunol. 1999;163(9):4833-41.
14. Coury F, Zenger S, Stewart AK, Stephens S, Neff L, Tsang K, et al. SLC4A2-mediated Cl-/HCO3- exchange activity is essential for calpain-dependent regulation of the actin cytoskeleton in osteoclasts. Proc Natl Acad Sci U S A. 2013;110(6):2163-8.
15. Provot S, Kempf H, Murtaugh LC, Chung UI, Kim DW, Chyung J, et al. Nkx3.2/Bapx1 acts as a negative regulator of chondrocyte maturation. Development. 2006;133(4):651-62.
16. Tribioli C, Lufkin T. The murine Bapx1 homeobox gene plays a critical role in embryonic development of the axial skeleton and spleen. Development. 1999;126(24):5699-711.
17. Pickering C, Hagglund M, Szmydynger-Chodobska J, Marques F, Palha JA, Waller L, et al. The Adhesion GPCR GPR125 is specifically expressed in the choroid plexus and is upregulated following brain injury. BMC Neurosci. 2008;9:97.
18. Liu C, Li S, Liu T, Borjigin J, Lin JD. Transcriptional coactivator PGC-1alpha integrates the mammalian clock and energy metabolism. Nature. 2007;447(7143):477-81.

19. Miettinen HE, Rayburn H, Krieger M. Abnormal lipoprotein metabolism and reversible female infertility in HDL receptor (SR-BI)-deficient mice. J Clin Invest. 2001;108(11):1717-22.
20. Perkins CP, Mar V, Shutter JR, del Castillo J, Danilenko DM, Medlock ES, et al. Anemia and perinatal death result from loss of the murine ecotropic retrovirus receptor mCAT-1. Genes Dev. 1997;11(7):914-25.
21. Bladt F, Riethmacher D, Isenmann S, Aguzzi A, Birchmeier C. Essential role for the c-met receptor in the migration of myogenic precursor cells into the limb bud. Nature. 1995;376(6543):768-71.
22. Webster MT, Fan CM. c-MET regulates myoblast motility and myocyte fusion during adult skeletal muscle regeneration. PloS one. 2013;8(11):e81757.
23. Cryan JF, Kelly PH, Neijt HC, Sansig G, Flor PJ, van Der Putten H. Antidepressant and anxiolytic-like effects in mice lacking the group III metabotropic glutamate receptor mGluR7. The European journal of neuroscience. 2003;17(11):2409-17.
24. Saito T, Fukai A, Mabuchi A, Ikeda T, Yano F, Ohba S, et al. Transcriptional regulation of endochondral ossification by HIF-2alpha during skeletal growth and osteoarthritis development. Nat Med. 2010;16(6):678-86.
25. Shen JC, Loeb LA. The Werner syndrome gene: the molecular basis of RecQ helicase-deficiency diseases. Trends Genet. 2000;16(5):213-20.
26. Lebel M, Leder P. A deletion within the murine Werner syndrome helicase induces sensitivity to inhibitors of topoisomerase and loss of cellular proliferative capacity. Proc Natl Acad Sci U S A. 1998;95(22):13097-102.
27. Arimitsu N, Akimitsu N, Kotani N, Takasaki S, Kina T, Hamamoto H, et al. Glycophorin A requirement for expression of O-linked antigens on the erythrocyte membrane. Genes Cells. 2003;8(9):769-77.
28. Kennedy MK, Glaccum M, Brown SN, Butz EA, Viney JL, Embers M, et al. Reversible defects in natural killer and memory CD8 T cell lineages in interleukin 15-deficient mice. J Exp Med. 2000;191(5):771-80.
29. Li T, Xiao J, Wu Z, Qiu G. Over-expression of c-maf by chondrocytes in osteoarthritis. J Int Med Res. 2009;37(1):129-35.
30. MacLean HE, Kim JI, Glimcher MJ, Wang J, Kronenberg HM, Glimcher LH. Absence of transcription factor c-maf causes abnormal terminal differentiation of hypertrophic chondrocytes during endochondral bone development. Dev Biol. 2003;262(1):51-63.
31. Zhang XK, Moussa O, LaRue A, Bradshaw S, Molano I, Spyropoulos DD, et al. The transcription factor Fli-1 modulates marginal zone and follicular B cell development in mice. J Immunol. 2008;181(3):1644-54.
32. Yadav VK, Ryu JH, Suda N, Tanaka KF, Gingrich JA, Schutz G, et al. Lrp5 controls bone formation by inhibiting serotonin synthesis in the duodenum. Cell. 2008;135(5):825-37.
33. Brunner D, Buhot MC, Hen R, Hofer M. Anxiety, motor activation, and maternal-infant interactions in 5HT1B knockout mice. Behav Neurosci. 1999;113(3):587-601.

34. Brown SD, Moore MW. The International Mouse Phenotyping Consortium: past and future perspectives on mouse phenotyping. Mammalian genome : official journal of the International Mammalian Genome Society. 2012;23(9-10):632-40.
35. Watanabe A, Toyota T, Owada Y, Hayashi T, Iwayama Y, Matsumata M, et al. Fabp7 maps to a quantitative trait locus for a schizophrenia endophenotype. PLoS biology. 2007;5(11):e297.
36. Kudo T, Ikeda M, Nishikawa M, Yang Z, Ohno K, Nakagawa K, et al. The RASSF3 candidate tumor suppressor induces apoptosis and G1-S cell-cycle arrest via p53. Cancer Res. 2012;72(11):2901-11.
37. Chen X, Cao H, Saraf A, Zweifel LS, Storm DR. Overexpression of the type 1 adenylyl cyclase in the forebrain leads to deficits of behavioral inhibition. J Neurosci. 2015;35(1):339-51.
38. Lin H, Grosschedl R. Failure of B-cell differentiation in mice lacking the transcription factor EBF. Nature. 1995;376(6537):263-7.
39. Smith ML, Fornace AJ, Jr. Genomic instability and the role of p53 mutations in cancer cells. Curr Opin Oncol. 1995;7(1):69-75.
40. Bolanos-Garcia VM. Aurora kinases. Int J Biochem Cell Biol. 2005;37(8):1572-7.
41. Chan JY, Kwong M, Lu R, Chang J, Wang B, Yen TS, et al. Targeted disruption of the ubiquitous CNC-bZIP transcription factor, Nrf-1, results in anemia and embryonic lethality in mice. EMBO J. 1998;17(6):1779-87.
42. Koch MA, Tucker-Heard G, Perdue NR, Killebrew JR, Urdahl KB, Campbell DJ. The transcription factor T-bet controls regulatory T cell homeostasis and function during type 1 inflammation. Nat Immunol. 2009;10(6):595-602.
43. Szabo SJ, Sullivan BM, Stemmann C, Satoskar AR, Sleckman BP, Glimcher LH. Distinct effects of T-bet in TH1 lineage commitment and IFN-gamma production in CD4 and CD8 T cells. Science. 2002;295(5553):338-42.
44. Galea GL, Meakin LB, Williams CM, Hulin-Curtis SL, Lanyon LE, Poole AW, et al. Protein kinase Calpha (PKCalpha) regulates bone architecture and osteoblast activity. J Biol Chem. 2014;289(37):25509-22.
45. Cannarile MA, Lind NA, Rivera R, Sheridan AD, Camfield KA, Wu BB, et al. Transcriptional regulator Id2 mediates CD8+ T cell immunity. Nat Immunol. 2006;7(12):1317-25.
46. Kostin S, Hein S, Arnon E, Scholz D, Schaper J. The cytoskeleton and related proteins in the human failing heart. Heart Fail Rev. 2000;5(3):271-80.
47. Lange M, Kaynak B, Forster UB, Tonjes M, Fischer JJ, Grimm C, et al. Regulation of muscle development by DPF3, a novel histone acetylation and methylation reader of the BAF chromatin remodeling complex. Genes Dev. 2008;22(17):2370-84.
48. Abe E, Marians RC, Yu W, Wu XB, Ando T, Li Y, et al. TSH is a negative regulator of skeletal remodeling. Cell. 2003;115(2):151-62.
49. Stengel PW, Yamada M, Wess J, Cohen ML. M(3)-receptor knockout mice: muscarinic receptor function in atria, stomach fundus, urinary bladder, and trachea. Am J Physiol Regul Integr Comp Physiol. 2002;282(5):R1443-9.

50. Matzuk MM, Lu N, Vogel H, Sellheyer K, Roop DR, Bradley A. Multiple defects and perinatal death in mice deficient in follistatin. Nature. 1995;374(6520):360-3.
51. Lee SJ, Lee YS, Zimmers TA, Soleimani A, Matzuk MM, Tsuchida K, et al. Regulation of muscle mass by follistatin and activins. Mol Endocrinol. 2010;24(10):1998-2008.
52. Hoshina N, Tanimura A, Yamasaki M, Inoue T, Fukabori R, Kuroda T, et al. Protocadherin 17 regulates presynaptic assembly in topographic corticobasal Ganglia circuits. Neuron. 2013;78(5):839-54.
53. Munoz-Bravo JL, Hidalgo-Figueroa M, Pascual A, Lopez-Barneo J, Leal-Cerro A, Cano DA. GDNF is required for neural colonization of the pancreas. Development. 2013;140(17):3669-79.
54. Matsukawa N, Grzesik WJ, Takahashi N, Pandey KN, Pang S, Yamauchi M, et al. The natriuretic peptide clearance receptor locally modulates the physiological effects of the natriuretic peptide system. Proc Natl Acad Sci U S A. 1999;96(13):7403-8.
55. Chen J, Tu X, Esen E, Joeng KS, Lin C, Arbeit JM, et al. WNT7B promotes bone formation in part through mTORC1. PLoS genetics. 2014;10(1):e1004145.
56. Tu X, Joeng KS, Nakayama KI, Nakayama K, Rajagopal J, Carroll TJ, et al. Noncanonical Wnt signaling through G protein-linked PKCdelta activation promotes bone formation. Dev Cell. 2007;12(1):113-27.
57. Laird PW, van der Lugt NM, Clarke A, Domen J, Linders K, McWhir J, et al. In vivo analysis of Pim-1 deficiency. Nucleic acids research. 1993;21(20):4750-5.
58. Haziza S, Magnani R, Lan D, Keinan O, Saada A, Hershkovitz E, et al. Calmodulin Methyltransferase Is Required for Growth, Muscle Strength, Somatosensory Development and Brain Function. PLoS genetics. 2015;11(8):e1005388.
59. Taniguchi K, Ayada T, Ichiyama K, Kohno R, Yonemitsu Y, Minami Y, et al. Sprouty2 and Sprouty4 are essential for embryonic morphogenesis and regulation of FGF signaling. Biochem Biophys Res Commun. 2007;352(4):896-902.
60. Bergqvist I, Eriksson M, Saarikettu J, Eriksson B, Corneliussen B, Grundstrom T, et al. The basic helix-loop-helix transcription factor E2-2 is involved in T lymphocyte development. Eur J Immunol. 2000;30(10):2857-63.
61. Seo KW, Wang Y, Kokubo H, Kettlewell JR, Zarkower DA, Johnson RL. Targeted disruption of the DM domain containing transcription factor Dmrt2 reveals an essential role in somite patterning. Dev Biol. 2006;290(1):200-10.
62. Lee JM, Park H, Noh AL, Kang JH, Chen L, Zheng T, et al. 5-Lipoxygenase mediates RANKL-induced osteoclast formation via the cysteinyl leukotriene receptor 1. J Immunol. 2012;189(11):5284-92.

Supplementary Table 7

sig	logP	N	v	power
0.5	4.18	1000	0.005	0.040
0.5	4.18	1000	0.01	0.203
0.5	4.18	1000	0.016	0.513
0.5	4.18	1000	0.02	0.684
0.5	4.18	1732	0.005	0.147
0.5	4.18	1732	0.01	0.567
0.5	4.18	1732	0.016	0.904
0.5	4.18	1732	0.02	0.971
0.5	4.18	2000	0.005	0.203
0.5	4.18	2000	0.01	0.684
0.5	4.18	2000	0.016	0.955
0.5	4.18	2000	0.02	0.990
0.5	4.18	4000	0.005	0.684
0.5	4.18	4000	0.01	0.990
0.5	4.18	4000	0.016	1.000
0.5	4.18	4000	0.02	1.000
0.9	5.06	1000	0.005	0.013
0.9	5.06	1000	0.01	0.099
0.9	5.06	1000	0.016	0.336
0.9	5.06	1000	0.02	0.510
0.9	5.06	1732	0.005	0.066
0.9	5.06	1732	0.01	0.387
0.9	5.06	1732	0.016	0.802
0.9	5.06	1732	0.02	0.925
0.9	5.06	2000	0.005	0.099
0.9	5.06	2000	0.01	0.510
0.9	5.06	2000	0.016	0.893
0.9	5.06	2000	0.02	0.970
0.9	5.06	4000	0.005	0.510
0.9	5.06	4000	0.01	0.970
0.9	5.06	4000	0.016	1.000
0.9	5.06	4000	0.02	1.000
0.95	5.39	1000	0.005	0.009
0.95	5.39	1000	0.01	0.074
0.95	5.39	1000	0.016	0.281
0.95	5.39	1000	0.02	0.447
0.95	5.39	1732	0.005	0.048
0.95	5.39	1732	0.01	0.328
0.95	5.39	1732	0.016	0.755
0.95	5.39	1732	0.02	0.900
0.95	5.39	2000	0.005	0.074
0.95	5.39	2000	0.01	0.447
0.95	5.39	2000	0.016	0.861
0.95	5.39	2000	0.02	0.957
0.95	5.39	4000	0.005	0.447
0.95	5.39	4000	0.01	0.957
0.95	5.39	4000	0.016	1.000
0.95	5.39	4000	0.02	1.000

Supplementary Figure 1

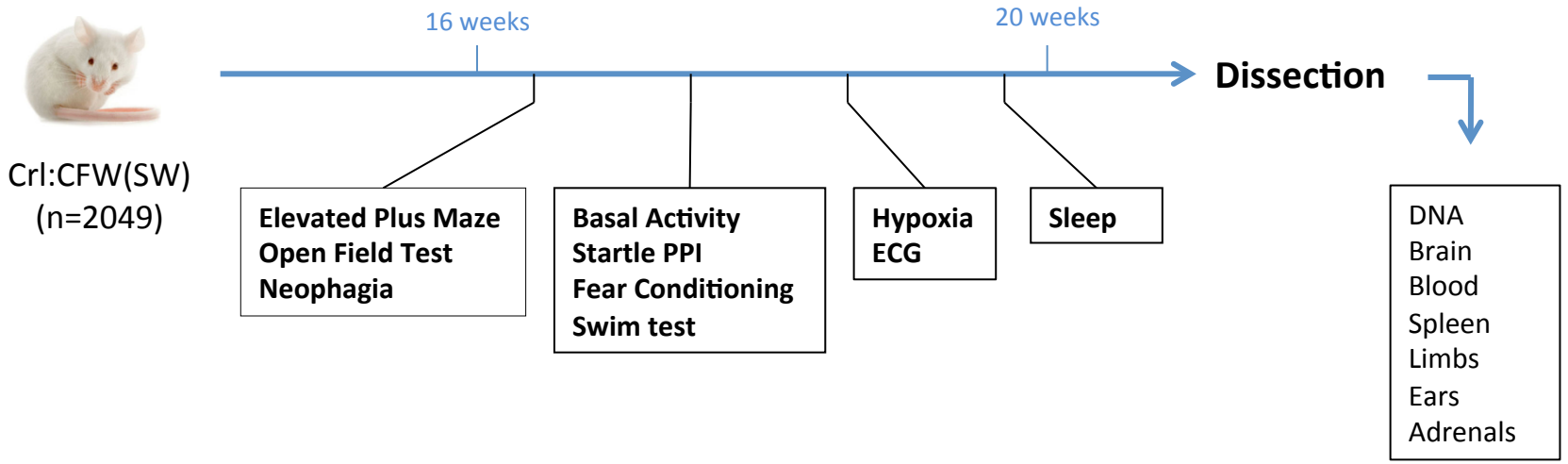

Supplementary Figure 2

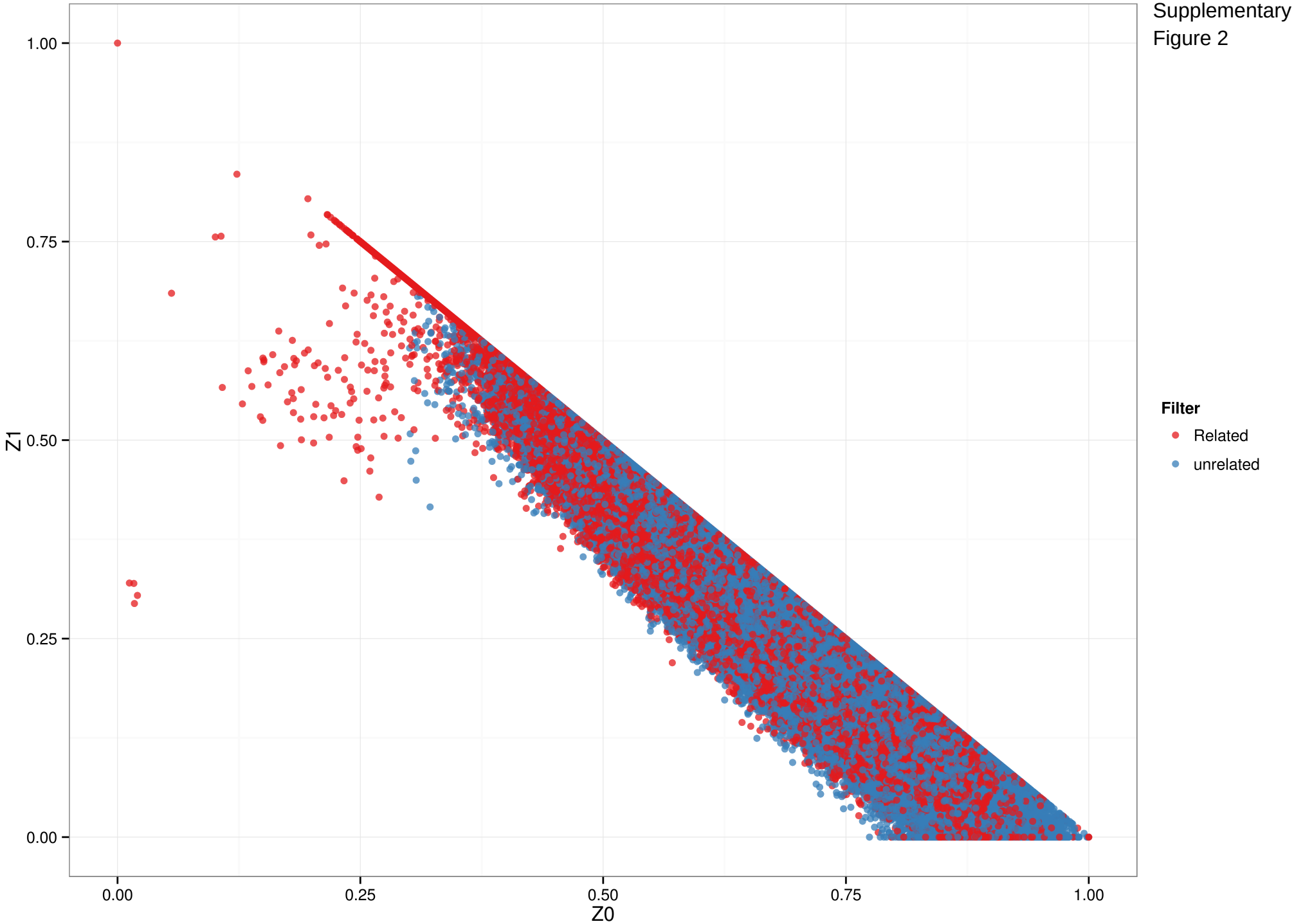

Supplementary Figure 3

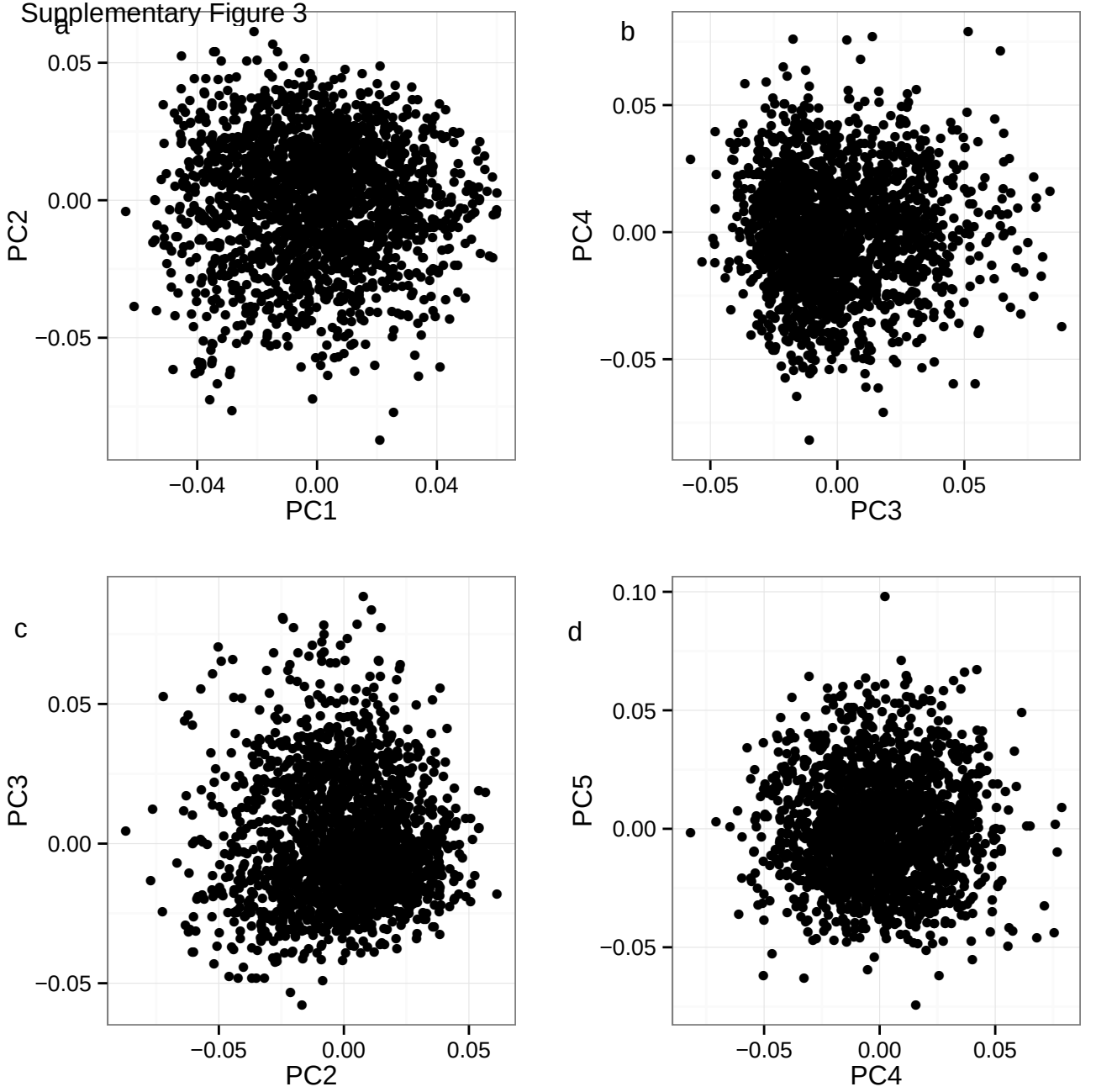

Supplementary Figure 4

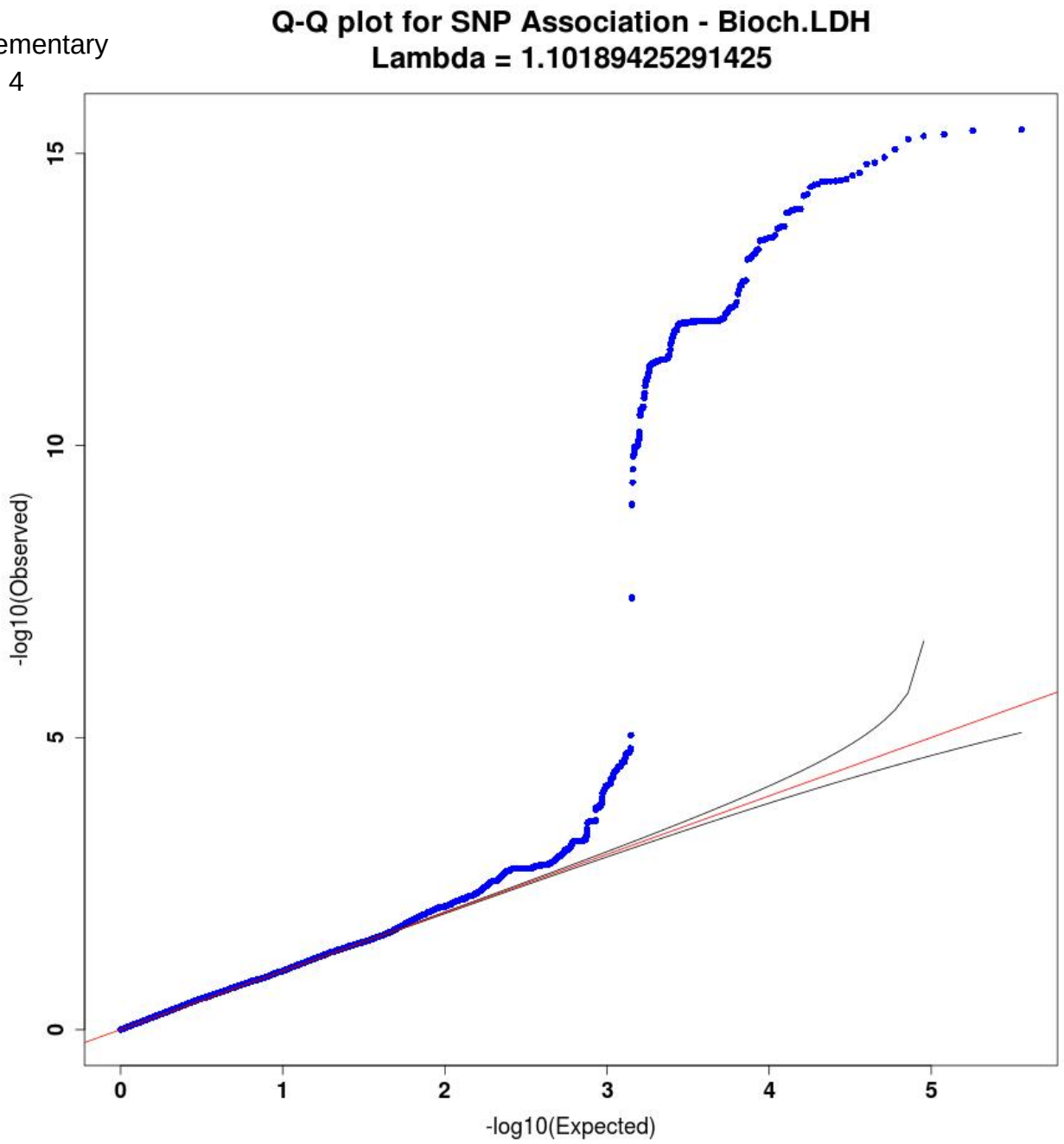

Supplementary Figure 4

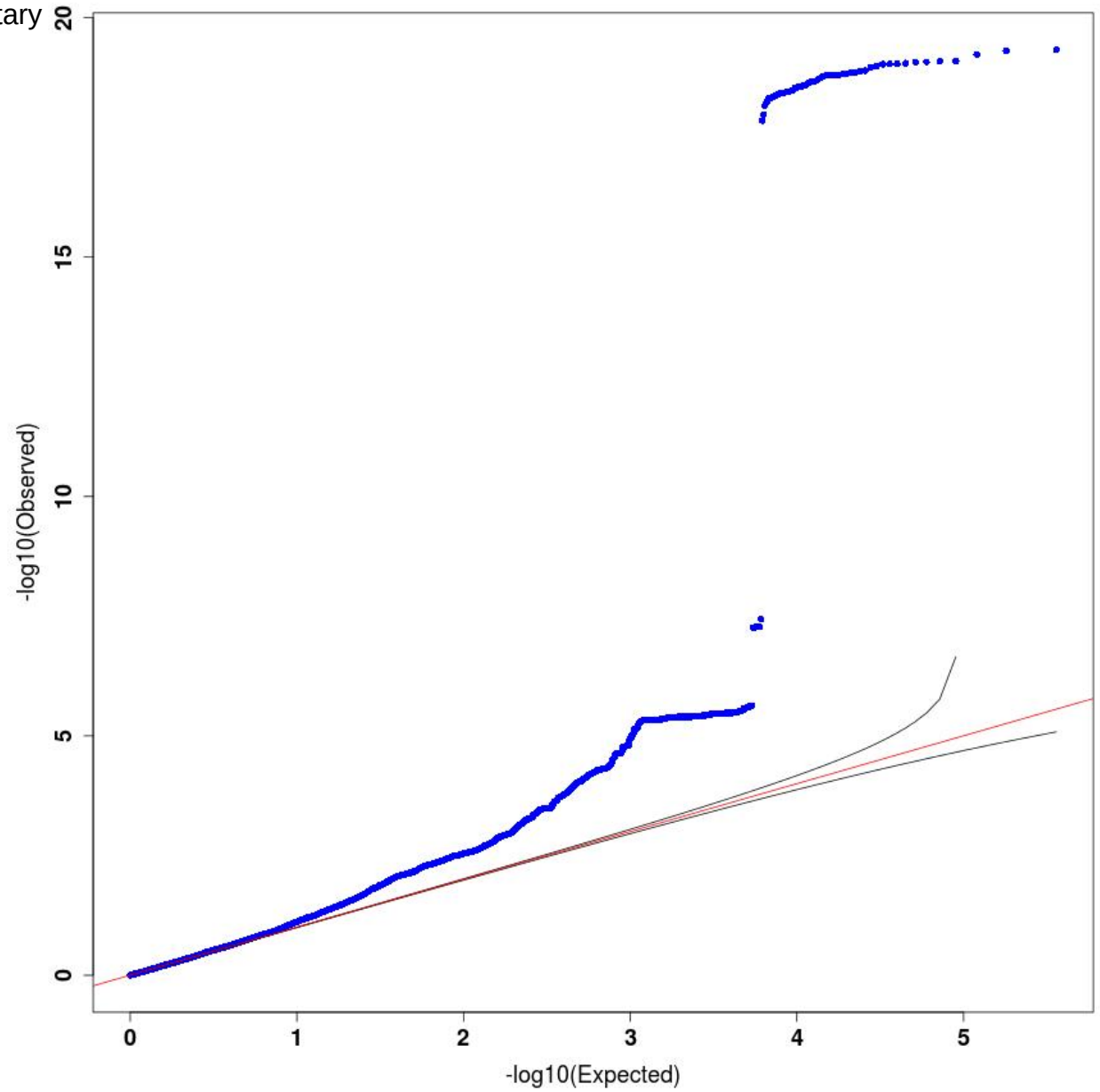

Supplementary Figure 4

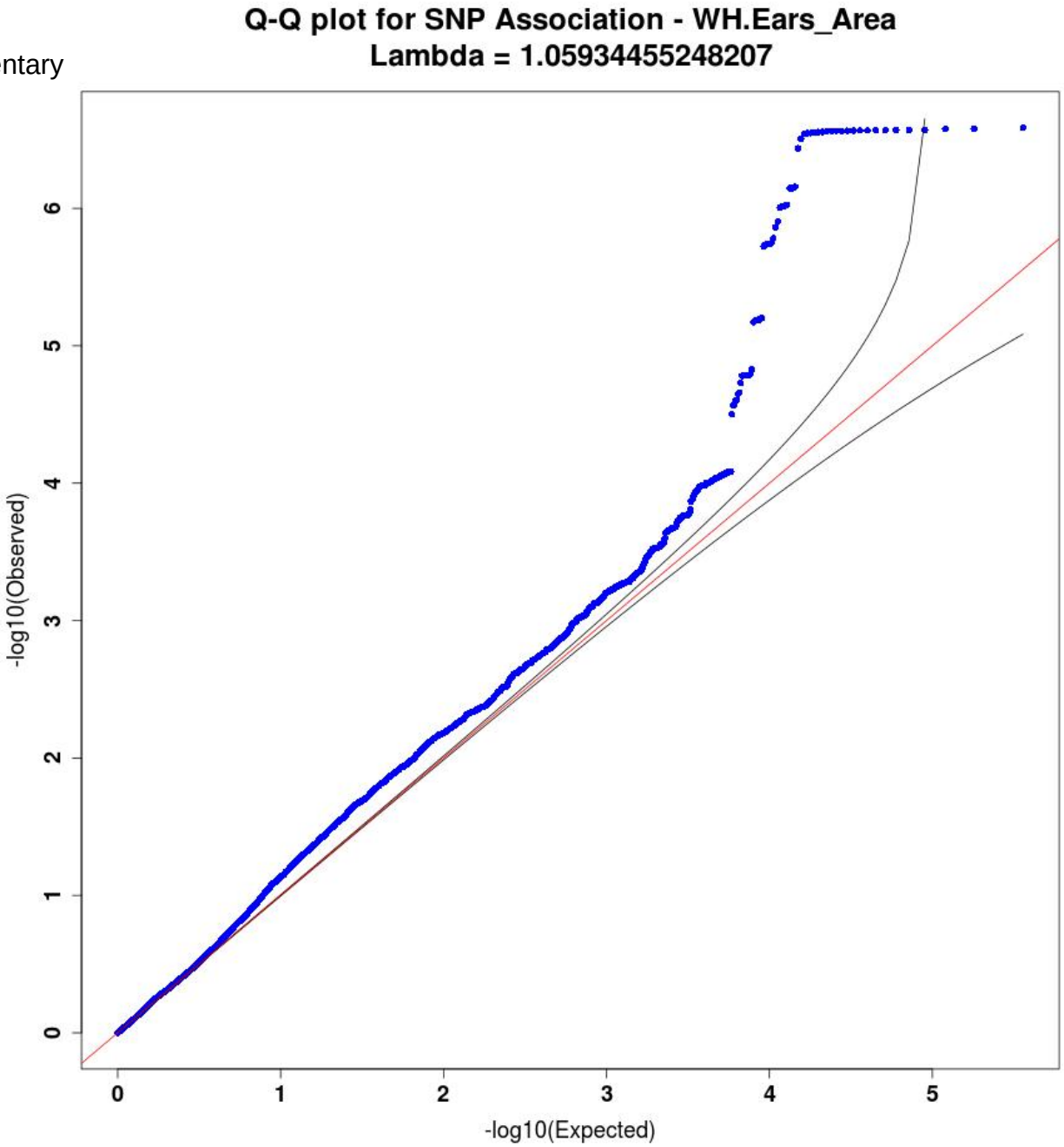

Supplementary Figure 4

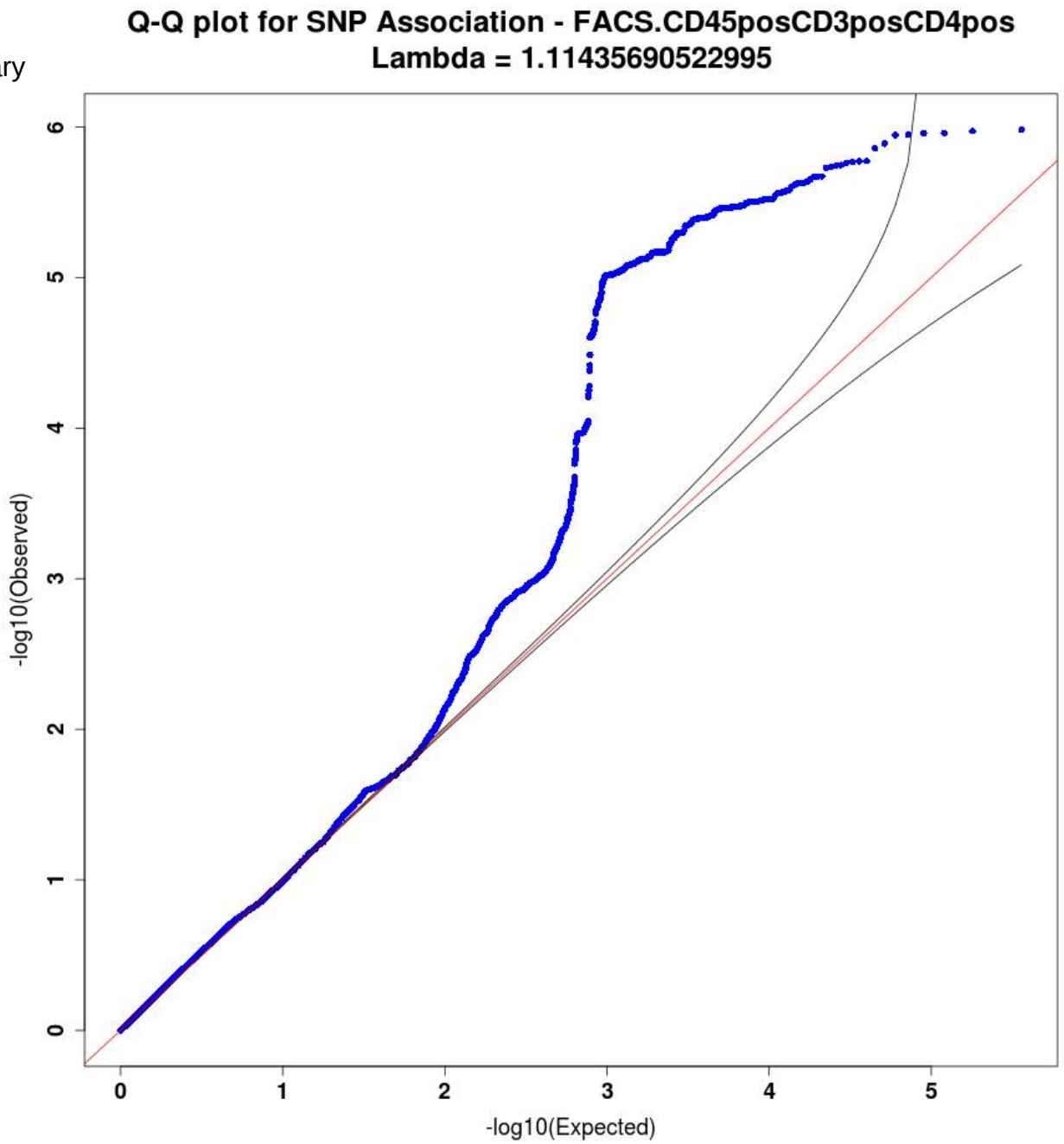

Supplementary Figure 4

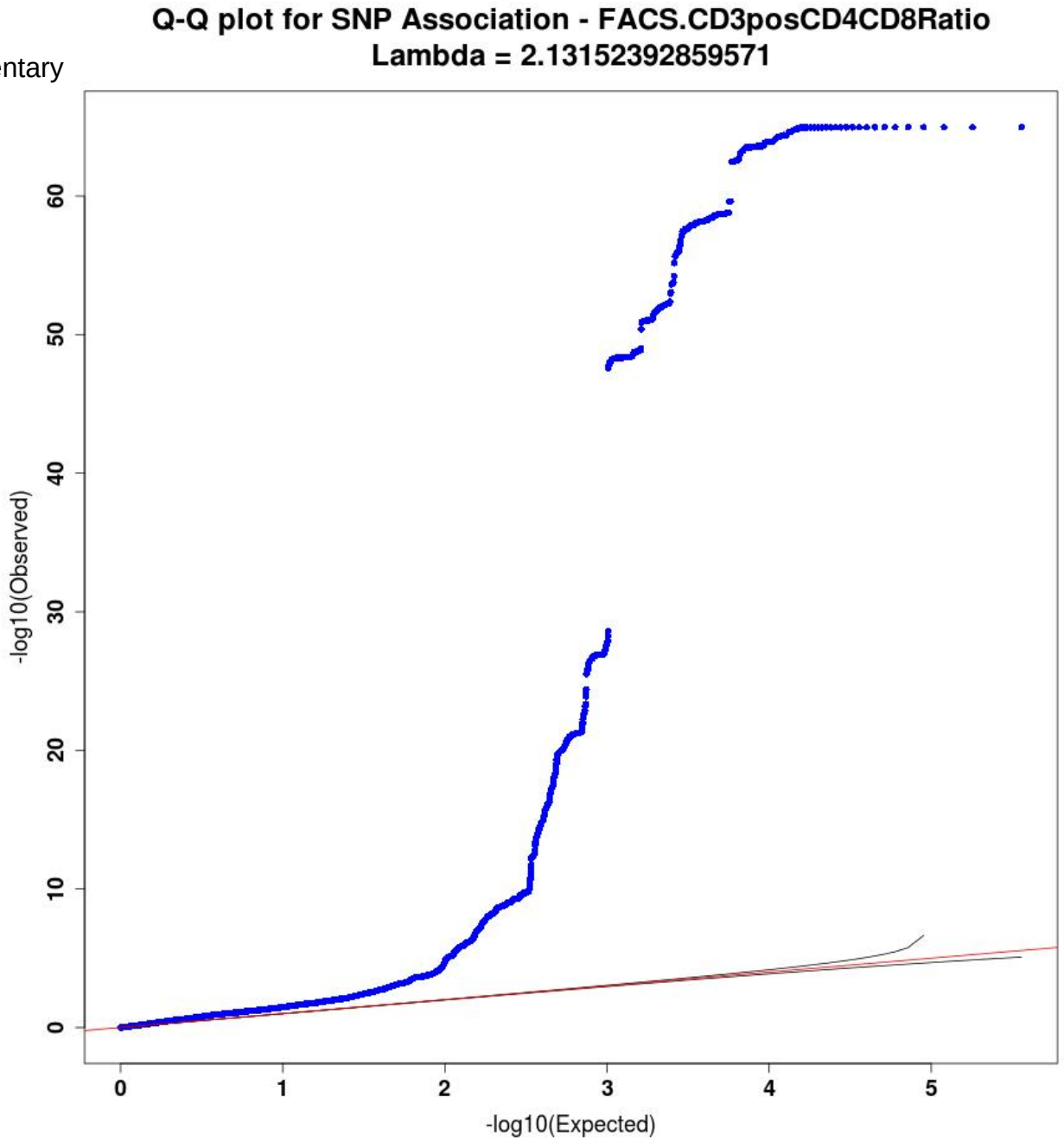

Supplementary Figure 4

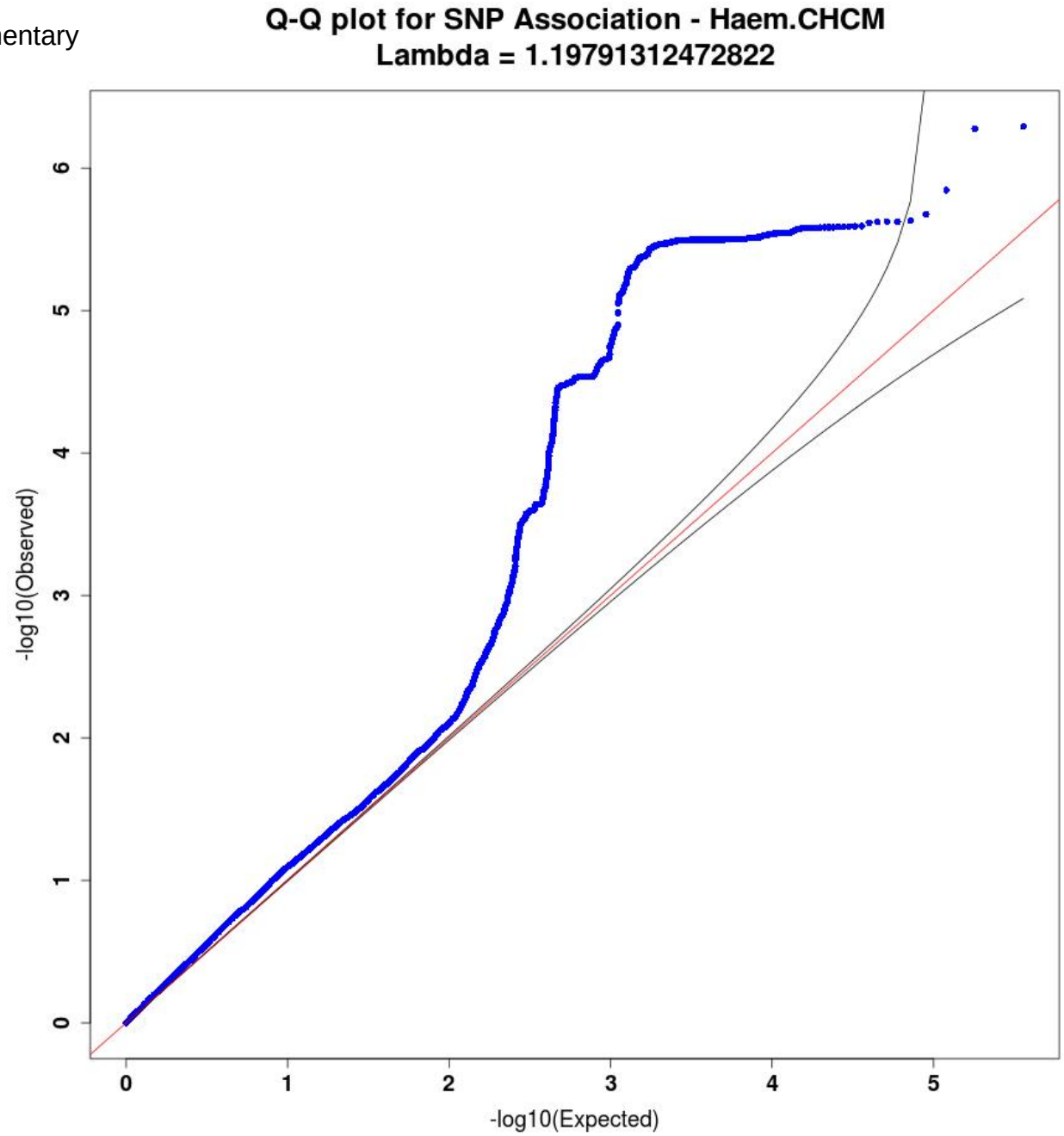

Supplementary Figure 4

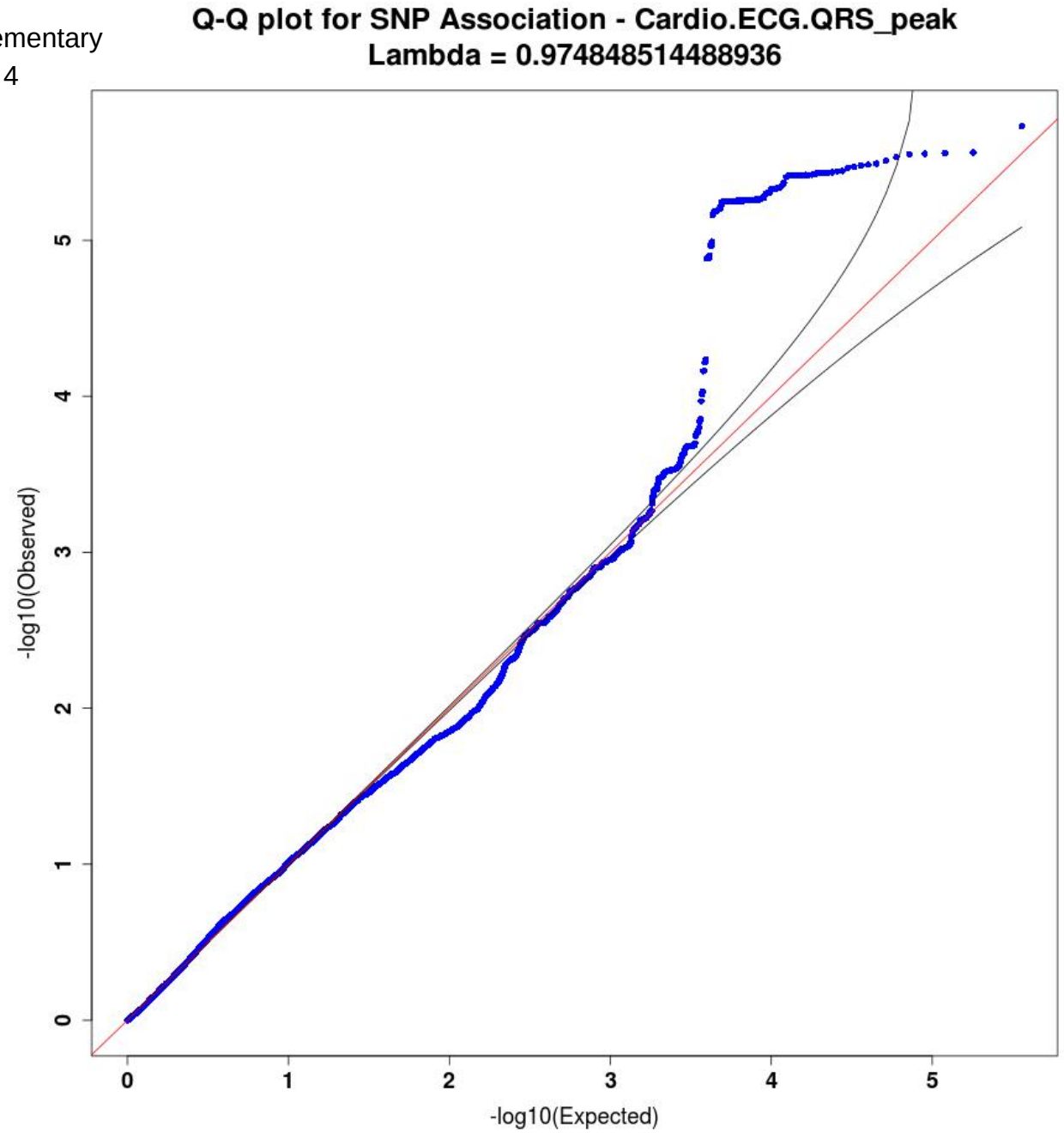

Supplementary Figure 4

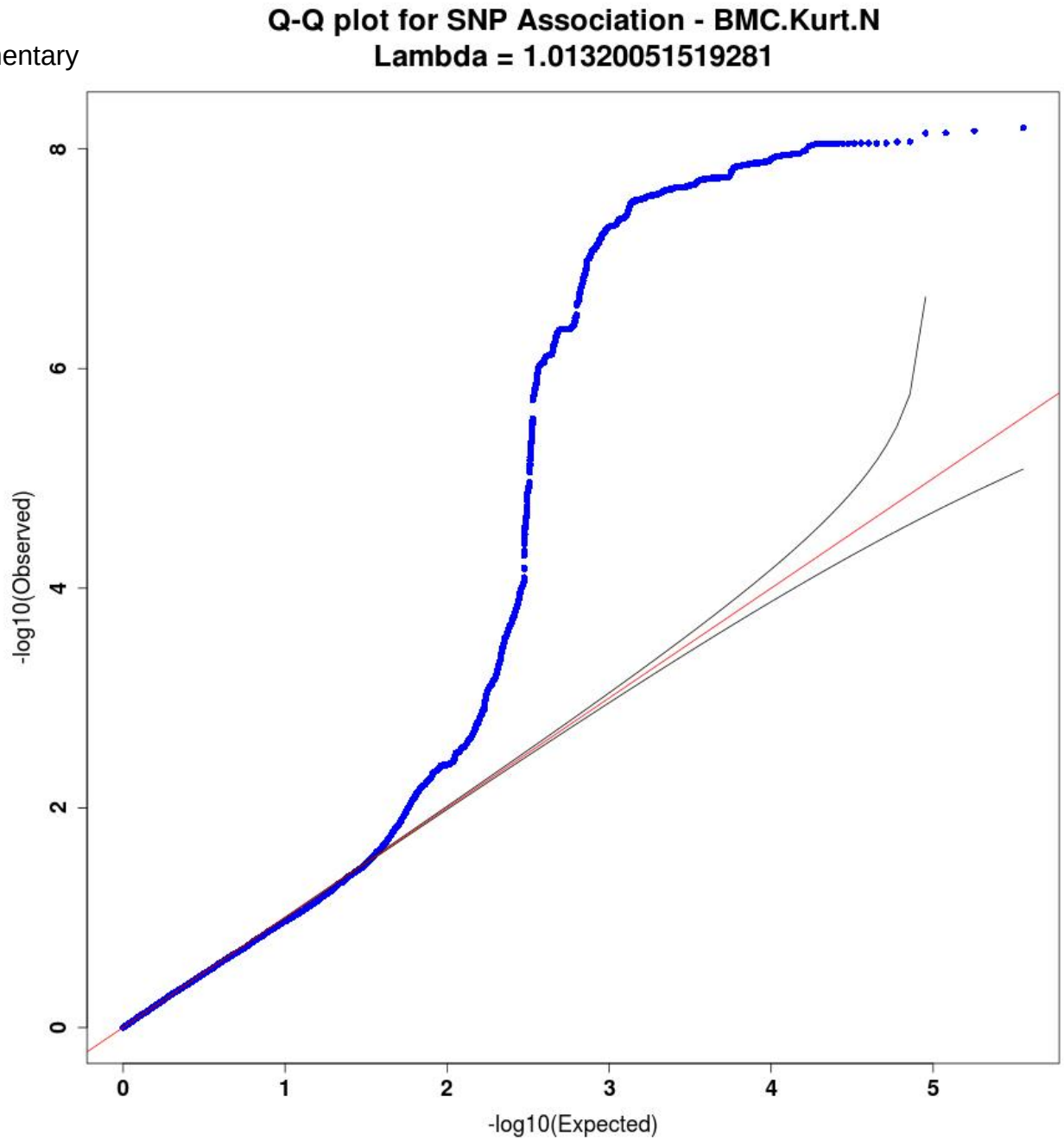

Supplementary Figure 4

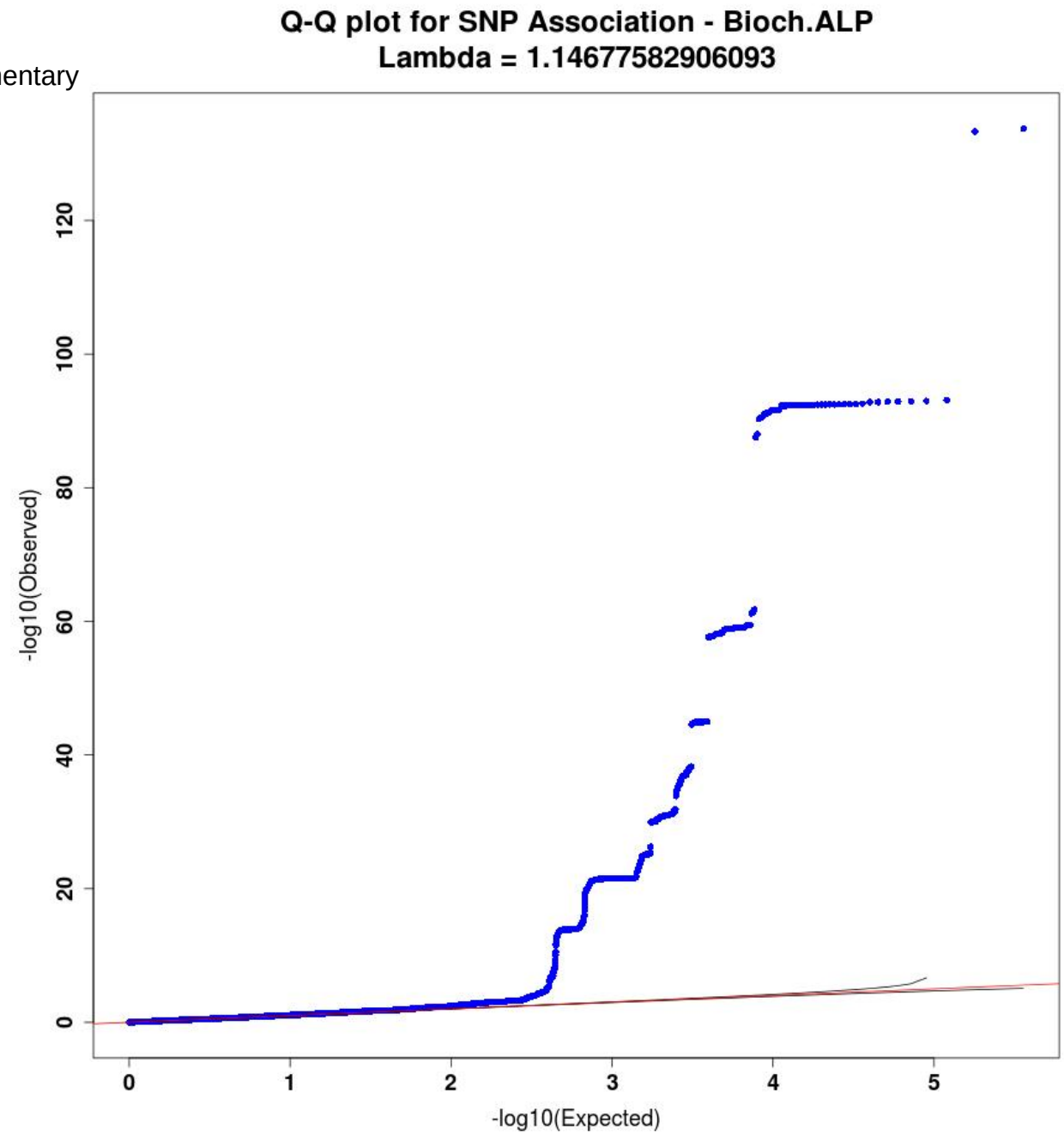

Supplementary Figure 4